

Comparison of Refractive-Index Sensitivities of Optical-Mode Resonances on a Finite Comb-Like Grating of Silver Nanostrips

Olga V. Shapoval, *Member, IEEE*

Abstract—We investigate the interplay of several different types of resonances in the scattering of light by finite comb-like nanogratings made of silver strips, in the H- and E-polarization cases. The resonances studied correspond to the localized surface plasmon modes, the periodicity-induced grating mode, and the cavity modes. They show up as Fano shapes in the total scattering cross sections and absorption cross sections. We find that the grating-mode and the cavity-mode resonances have higher values of both bulk refractive-index sensitivity and figure-of-merit than the localized-surface-plasmon resonances, in the visible band.

Index Terms—Comb-like strip gratings, resonance, refractive-index sensitivity, figure-of-merit.

I. INTRODUCTION

OPTICAL resonances on nanogratings of noble-metal elements are important topic of today's research because of potential applications in nanoscale optical biosensing, photovoltaics, and nanoelectronics. As known, they display intensive localized surface-plasmon (LSP) resonances in the visible-light and infrared ranges controlled by the nanoparticle shape [1]–[3]. One of the main areas of their applications is LSP biochemical sensors of the host medium refractive index [4], [5]. Besides, if sub-wavelength metal particles, strips or wires are collected into large enough periodic arrays, they display extraordinarily large reflection, absorption, and near-field enhancement at certain wavelengths depending on the period, angle of incidence and host medium refractive index. These phenomena are caused by the so-called grating-mode (GM, a.k.a. lattice, collective, and geometrical) resonances [6]–[22] which appear due to periodicity [20]–[22]. Recently biosensors based on the GM resonances started attracting increased attention [17]. This is because their Q-factors can be large [18] and their sensitivities do not depend on the refractive index of the host medium and are proportional to the period. Still besides, in thicker gratings, interaction between adjacent elements can lead to appearance of so-called cavity-mode (CM, a.k.a gap and slot) resonances [2].

Manuscript received January 5, 2015; revised January 29, 2015; accepted February 2, 2015. Date of publication February 18, 2015; date of current version February 26, 2015. This work was supported by the National Academy of Sciences of Ukraine through the State Target Program within the Nanotechnologies and Nanomaterials.

The author is with the Laboratory of Micro and Nano Optics, Institute of Radio-Physics and Electronics, National Academy of Sciences of Ukraine, Kharkiv 61000, Ukraine (e-mail: olga.v.shapoval@gmail.com).

Color versions of one or more of the figures in this paper are available online at <http://ieeexplore.ieee.org>.

Digital Object Identifier 10.1109/JQE.2015.2404785

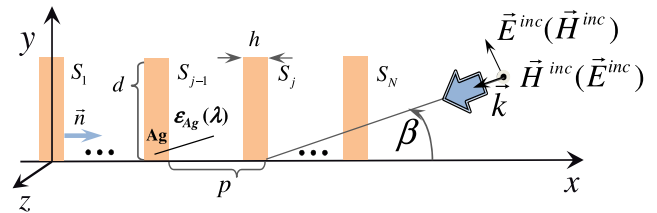


Fig. 1. Cross-section of a free-standing comb-like finite nanostrip grating of N infinitely long (along z -axis) noble-metal strips.

In this paper we present an accurate numerical analysis of the optical response of finite comb-like silver strip gratings in the visible range and compare the host medium refractive-index sensitivities and figures-of-merit of all associated resonances.

The remainder of the paper is structured as follows. In Section II, we present briefly the main points of our numerical method. Sections III and IV contain the numerical results related to the cases of H- and E-polarization, respectively. Section V deals with sensitivities and figures-of-merit of all H-case resonances. Conclusions are given in Section VI.

II. NUMERICAL METHOD: GENERALIZED BOUNDARY CONDITIONS AND NYSTROM-TYPE DISCRETIZATION

We consider the 2-D scattering of the H- and E-polarized plane waves by a comb-like finite grating of N identical silver nanostrips of the width d and thickness h (see Fig. 1) characterized by refractive index $\nu_{Ag} = \epsilon_{Ag}^{1/2}(\lambda)$, where ϵ_{Ag} is the complex-valued dielectric permittivity depending on the free-space wavelength λ . (see Appendix A1). The grating has period p and is placed into a host medium with refractive index ν_{host} . Note that for a nanostrip with thickness larger than a few nanometers one can neglect all non-local effects [23] and use experimental data of the bulk silver index ν_{Ag} [24].

As a reliable instrument for the modeling of the scattering and the resonance effects we use the previously developed [19], [25] median-line singular integral equation (SIE) method based on the two-side generalized boundary condition (GBC) [26], [27] and a Nystrom-type discretization [19], [28]. The use of GBC is justified by the fact that if the material layer thickness makes a small fraction of the wavelength ($h \ll \lambda$) then the electromagnetic

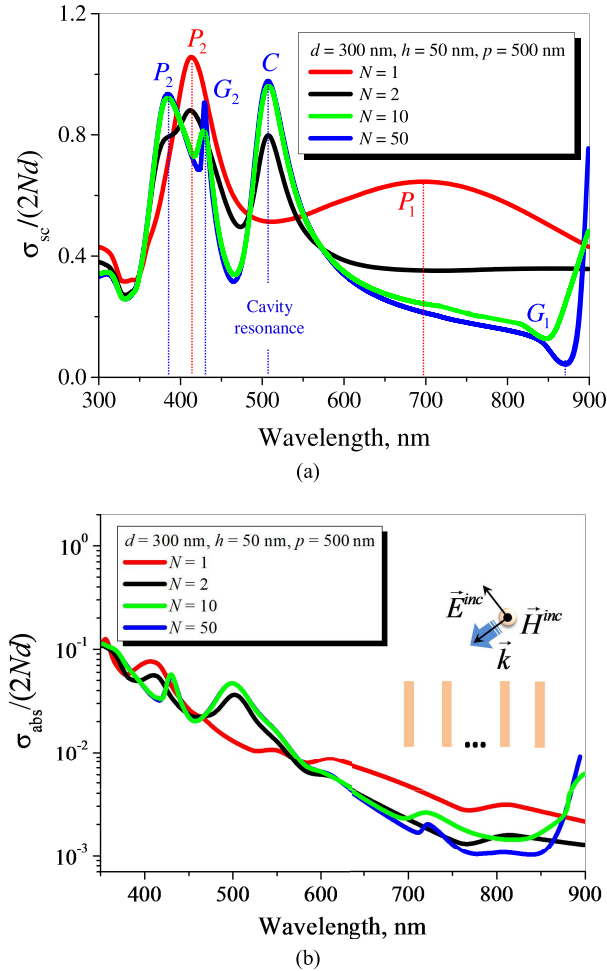


Fig. 2. H-polarization. Normalized TSCS (a) and ACS (b) for the gratings of $N = 1, 2, 10$ and 50 silver strips in free space ($v_{host} = 1$) at the inclined incidence of plane wave ($\beta = 45^\circ$).

analysis can be simplified by neglecting the field inside the layer and considering only the external field limiting values. If used in the comb-like grating scattering analysis, GBC leads to a set of the coupled SIEs with the strip median lines being the intervals of integration [29]. Such SIEs can be solved by various numerical techniques. We apply Nystrom-type method based on the interpolation polynomials for the unknown functions and the quadrature formulas, which guarantee the convergence of computations – see [25], [28], [29]. In our analysis the accuracy of computing the near and far-field data was kept at 10^{-4} or better.

III. H-POLARIZATION CASE

A. Interplay of Resonances: Localized Surface Plasmons, Grating Modes and Cavity Modes

To observe the optical resonances of all possible types of symmetry, we will show and discuss at first the spectra of the normalized by $2Nd$ total scattering cross-section (TSCS) and the absorption cross-section (ACS) for the plane wave illuminating the comb-like grating under the inclined incidence ($\beta = 45^\circ$, Fig. 2). This is because the spectra at the normal incidence ($\beta = 90^\circ$) and the grazing incidence ($\beta = 0$) reveal only part of them. Here, host medium is free space, $v_{host} = 1$.

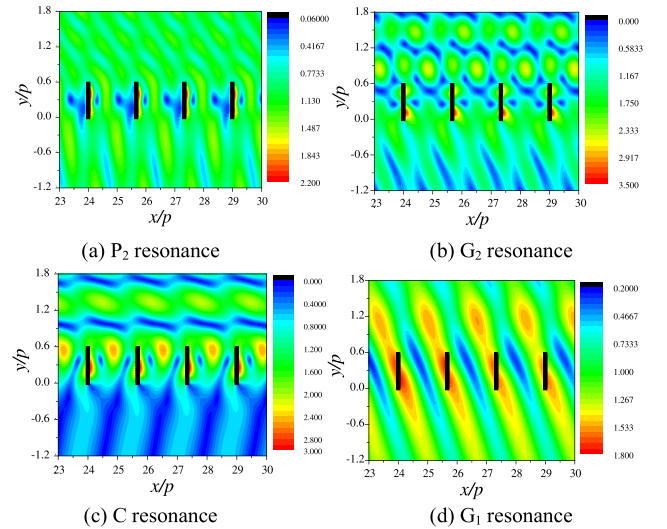


Fig. 3. In-resonance magnetic near-field patterns for $N = 50$ around four central strips at 384.2 nm (a), 428.7 nm (b), 506.5 nm (c) and 858.3 nm (d).

As one can see, for a stand-alone 300×50 nm² silver strip ($N = 1$) two optical LSP modes of the first and the second orders are observed in the visible band (red curves) at the resonance wavelengths $\lambda_{P_1} = 697.5$ nm and $\lambda_{P_2} = 413.2$ nm. If the strips are two ($N = 2$), the scattering spectrum keeps certain features characteristic for the single strip: the second-order optical LSP resonance is only slightly deformed and the first-order optical LSP resonance becomes less visible (twice lower in amplitude) because of the shadowing of the left strip by the right one.

However the spectra for $N = 2$ display something new: a strong resonance peak at the wavelength of $\lambda \approx 507$ nm. This new feature is kept almost intact if the number N is taken larger. This allows to conclude that this is a CM-resonance associated with the so-called “cavity mode” or “gap plasmon mode” between adjacent strips, which have width $d > \lambda/2$ [2].

Collecting more strips into a comb-like grating with period of $p = 500$ nm brings still new features to the visible-range response. As known [6]–[22], the periodicity leads to the appearance of specific GM-resonances on the grating modes. As shown in [18], their complex wavelengths $\lambda_{\pm m}^G$ are slightly up-shifted from the Rayleigh anomalies (RA) $\lambda_{\pm m}^{R.A.}$ of the associated infinite gratings [30],

$$\lambda_{\pm m}^G = \lambda_{\pm m}^{R.A.} (1 + \delta_{\pm m}), \quad |\delta_{\pm m}| \ll 1, \quad \text{Re} \delta_{\pm m} > 0 \quad (1)$$

$$\lambda_{\pm m}^{R.A.} = v_{host} (p/m) (1 \mp \cos \beta), \quad m = 1, 2, 3 \dots \quad (2)$$

Note that, if $\beta = 45^\circ$, then even a grating of only $N = 50$ strips displays a quite pronounced optical GM-resonance around $\lambda \approx 428$ nm. This is the vicinity of the $+2$ -nd RA at $\beta = 45^\circ$. Similarly, the extreme-red resonance appearing at $\lambda \geq 890$ nm corresponds to the $+1$ -st RA.

The in-resonance near-field patterns of $|H_z|$ in Fig. 3 show the area around four central strips of the $N = 50$ grating at $\lambda_{P_2} = 384.2$ nm (a), $\lambda_{G_2} = 428.7$ nm (b), $\lambda_C = 506.5$ nm (c) and $\lambda_{G_1} = 858.3$ nm (d). Note that optical LSP resonance P_2 is formed as a Fabry-Perot like standing wave due to the reflections of the surface-plasmon natural wave of a silver

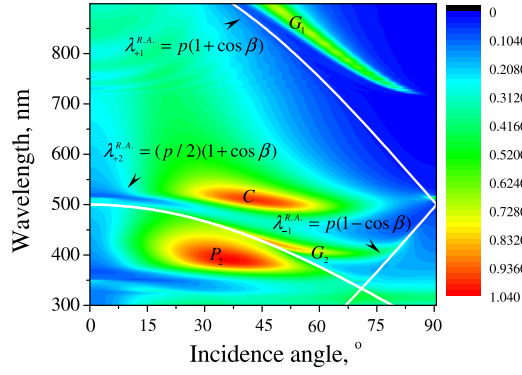


Fig. 4. H-polarization. Color-coded map of the normalized TSCS per one strip versus the wavelength and the incidence angle for the grating of $d = 300$ nm, $h = 50$ nm, $p = 500$ nm, and $N = 50$ ($v_{host} = 1$).

layer from the strip edges. Here, two half-wavelengths of the mentioned natural wave match the strip width (see Fig. 3(a)) and the hotspots of the LSP field are seen just at the strip faces.

In contrast, the near-field pattern in the CM-resonance (Fig. 3(c)) demonstrates bright spots in the space between the adjacent strips. Finally, the near-field patterns in the GM-resonances of 1st (Fig. 3(d)) and 2nd (Fig. 3(b)) order demonstrate still very different standing waves stretching far beyond the grating domain.

In order to bring together all discussed above resonance phenomena and see their dynamics at varying β , in Fig. 4 we show the color-coded map of TSCS (normalized by $2Nd$) as a function of two parameters: the wavelength and the incidence angle, for the grating of $N = 50$ strips of $d = 300$ nm, $h = 50$ nm and $p = 500$ nm. White curves indicate the RA values of the associated infinite grating, which are the functions of the anomaly index, m , and the angle β .

As one can see, there are several broad and narrow bright “ridges” in the visible range while β varies from 0 (grazing incidence) to 90° (normal incidence). Note that some of the ridges are extinct at $\beta = 0$ or 90° as their “parent” eigenmodes are orthogonal (of the opposite symmetry) to the incident plane wave coming along the x -axis or the y -axis, respectively.

The largest “mountain” between 375 nm and 450 nm corresponds to the second-order LSP mode P_2 on each silver strip of the comb-like grating. The other large “hill” around 510 nm corresponds to the mentioned above cavity mode C between each pair of adjacent strips. Note that the both resonances in the scattering cross-section die off at $\beta = 0$ and 90° (i.e. turn from bright to dark resonances) because of the above-mentioned orthogonality of the incident wave.

Besides, one can observe two narrow “ridges” stretching approximately along the three RA curves (above them) given by $\lambda_{\pm 1}^{R.A.} = p(1 \mp \cos \beta)$ and $\lambda_{+2}^{R.A.} = (p/2)(1 + \cos \beta)$. These “ridges” correspond to the high-Q resonances on the grating modes associated with the combination of the +2nd and -1st Floquet harmonics (note the avoided crossing behavior), and with the +1st Floquet harmonic, respectively.

Specific case of the plane-wave normal incidence ($\beta = 90^\circ$) is presented in detail in Fig. 5. Here, only one strong

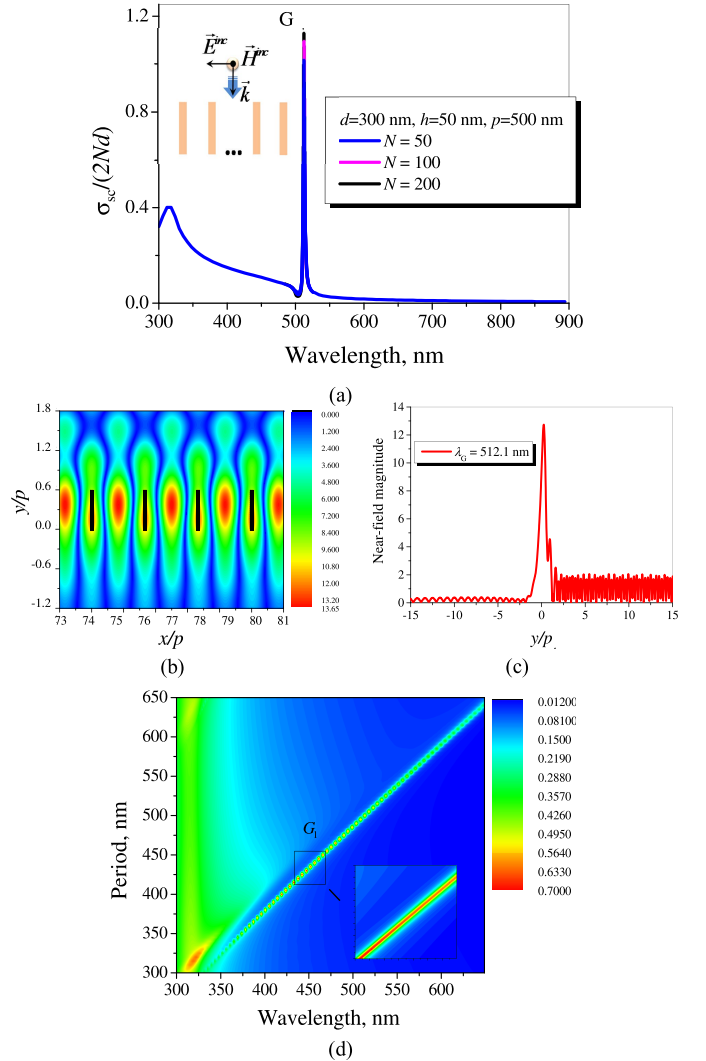


Fig. 5. H-polarization. (a) Normalized TSCS for the normally incident plane wave ($\beta = 90^\circ$) for the gratings of $N = 50, 100$ and 200 strips of $d = 300$ nm, $h = 50$ nm and $p = 500$ nm. (b) Magnetic near-field pattern in the GM-resonance at $\lambda_{G1} = 512.1$ nm. (c) Profile of the near field magnitude along the grating symmetry line, $x/p = 79.45$ in the GM-resonance. (d) Map of TSCS (in nm) versus the wavelength and the period for the grating of $N = 100$ strips with $d = 300$ nm and $h = 50$ nm.

GM resonance $G_{\pm 1}$ is visible at $\lambda_{G1} = 512.1$ nm. The in-resonance near-field profile along the normal to the grating (Fig. 5 (c)) shows that it reaches the magnitude 13.1 between the strips.

This is much larger than in the same GM resonance on a flat grating made of the same silver strips (studied in [19] and [22]).

The corresponding near-field pattern in Fig. 5 (b) shows the area around four central strips of the $N = 100$ grating (from #48 to #52). This pattern is strikingly different from the LSP-mode resonance: intensive standing wave appears along the grating with hotspots that stretch out far off the grating domain. It is built on the ± 1 -order Floquet harmonics along the grating.

On the color map of TSCS as a function of the wavelength and the period, at normal incidence (Fig. 5 (d)), one can see a sharp “ridge” stretching along the line $\lambda \approx p$ and another

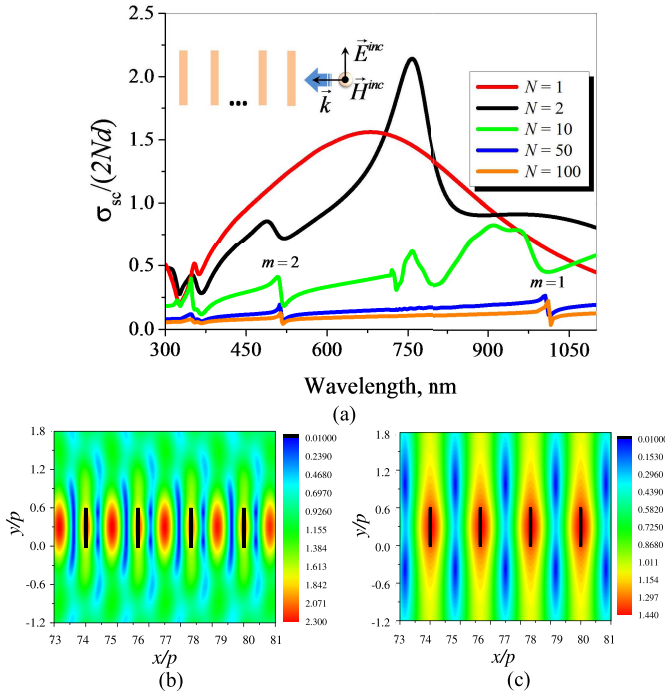


Fig. 6. H-polarization. (a) Normalized TSCS for the plane wave at the grazing incidence ($\beta = 0$) for the gratings of $N = 1, 2, 10, 50$ and 100 strips of $d = 300$ nm, $h = 50$ nm and $p = 500$ nm ($\nu_{host} = 1$). Total magnetic near-field patterns around four central strips at the wavelengths 515.8 nm (b) and 1016 nm (c) for the grating of $N = 50$ strips.

one between 300 nm and 350 nm. The former corresponds to the mentioned above GM with $m = \pm 1$ with the y -even field and the latter to the sister-mode with the y -odd field.

The case of the plane-wave grazing incidence ($\beta = 0$) is even more special because such incidence has no analog in the wave scattering by an infinite grating. Still one can see from eq. (2) and Fig. 4 that in such case one of RAs of any order $m = 1, 2, 3 \dots$ vanishes and the other tends to the value known as a Bragg's effect wavelength, $\lambda_m^{B.E.} = 2\nu_{host}(p/m)$ [31]. Indeed, at these values the spectra of the normalized TSCS show sharp double extrema (Fano-shape) resonances (see Fig. 6), the magnitudes of which decrease if N gets larger because of the shadowing of the rear strips by the front ones.

We present also the in-resonance magnetic near-field patterns visualized around four central strips from #25 to #28 at the wavelengths 515.8 nm (b) and 1016 nm (c) for the grating consisting of $N = 50$ strips. As one can see, here an integer number of the half-wavelengths stands between the strips, corresponding to the order of the Bragg's diffraction: $m = 2$ (b) and $m = 1$ (c), respectively.

IV. E-POLARIZATION CASE

In the E-polarization, as known, there are no optical LSP modes on metallic strips, and hence no associated resonances [1], [18], [22], [23]. As for the optical GM modes, they still exist as complex poles of the field as a function of the wavelength. However, their Q-factors are $|\epsilon_{Ag}|^2$ times smaller than in the H-polarization case [18] and therefore the associated resonances are not visible. Instead, if the

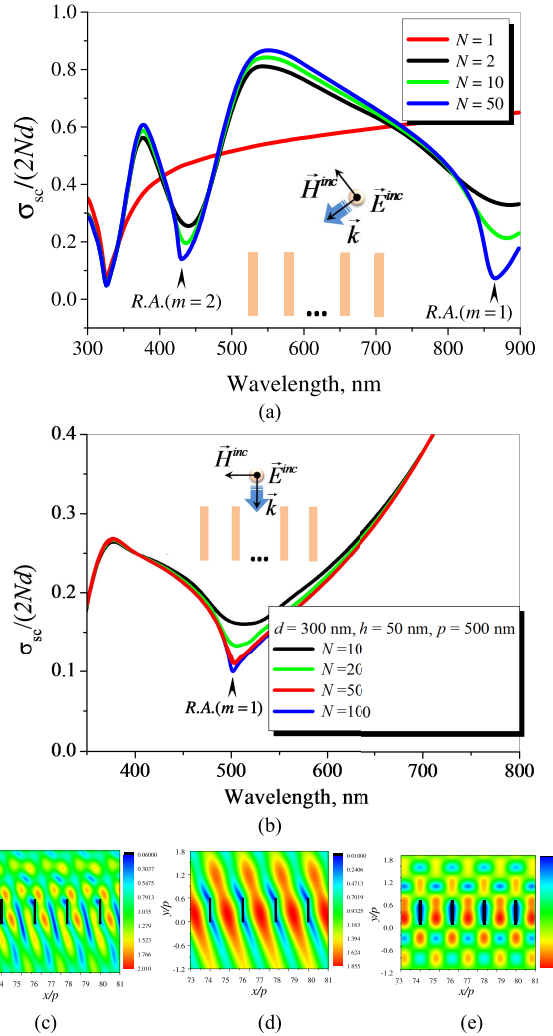


Fig. 7. E-polarization. (a) Normalized TSCS for the gratings of N strips of $d = 300$ nm, $h = 50$ nm and $p = 500$ nm ($\nu_{host} = 1$) at the inclined incidence of plane wave ($\beta = 45^\circ$). (b) The same at the normal incidence ($\beta = 90^\circ$). Electric near-field patterns at the wavelengths 430.3 nm (c) and 864.1 nm (d) for inclined incidence and 501.5 nm (e) for the normal incidence, $N = 50$.

number of strips N is increasing the build-up of Rayleigh anomalies is observed, accompanied by the reduced scattering and absorption.

We start again from the case of inclined incidence, $\beta = 45^\circ$, and show the spectra of the normalized TSCS in Fig. 7 (a). They reveal that two minima near to RA with $m = +1, +2$ appear already for $N = 2$. The same takes place at normal incidence ($\beta = 90^\circ$) however for $m = \pm 1$, see Fig. 7 (b).

The explanation of the scattering suppression becomes clear after visualizing the electric near-field patterns (Fig. 7 (c)-(e)) around four central strips from #25 to #28 at the wavelengths of the RA-related minima. Similarly to the RA scattering minima for a flat-strip grating (see [15]), the strips are located in the deep minima of the E-field and both scattering and absorption of the E-polarized plane wave get less intensive.

Finally, in Fig. 8 (a) we present the spectra of normalized TSCS for the grazing incidence ($\beta = 0$), for the same gratings.

The Bragg-effect Fano-shape resonances are observable at the wavelengths $\lambda_m^{B.E.}$ similarly to the H-case. The visualized near-field patterns at 346 nm (panel (b)), 510 nm (c) and

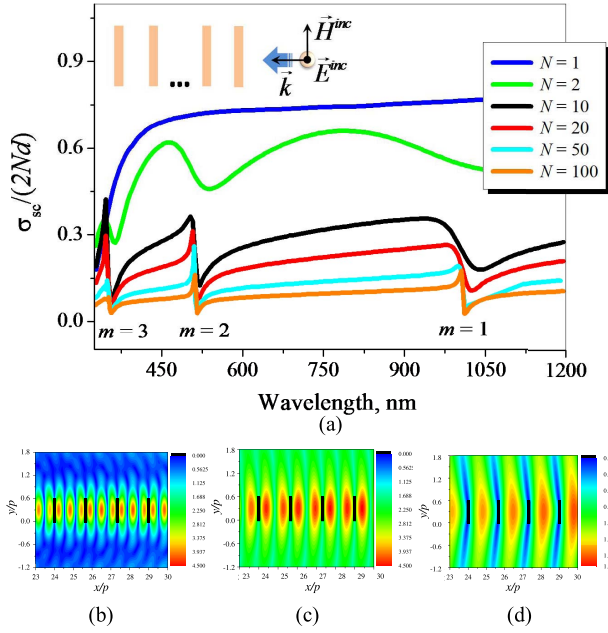


Fig. 8. E-polarization. (a) Normalized TSCS as a function of the wavelength for the gratings of $N = 1, 2, 10, 20, 50$ and 100 strips of $d = 300$ nm, $h = 50$ nm and $p = 500$ nm at the grazing incidence ($\beta = 0$). (b) Electric near-field patterns around four central strips from #25 to #28 at the wavelength 346 nm (b), 510 nm (c) and 1005 nm (d) for the grating of $N = 50$ strips.

1005 nm (d) for the grating of $N = 50$ strips are similar to the case of H-polarization (compare to Fig. 6 (b), (c)) however with deep E-field minima at the strip locations.

V. REFRACTIVE-INDEX SENSITIVITIES AND FOM

As already mentioned, noble-metal nanogratings attract the attention of researchers because of their high potential for applications in biological and chemical sensing. The physical mechanism that provides such opportunity is the dependence of the wavelength of an optical resonance peak in the scattering and absorption of light on the refractive index of the host medium [4]. Such sensors were at first designed on the LSP-resonances controlled by nanoparticle shape. The GM-resonances, which appear if the hundreds of metal particles are assembled in chains or arrays with good enough periodicity, were at first considered as a parasitic phenomenon. However, later the understanding has emerged that they are also very promising in the context of nanoscale biosensing [17], [32].

For metal nanogratings assembled of strips or wires, the optical LSP resonances exist only in the H-polarization and the GM resonances, albeit existing, are observable also only in this case because of high enough Q-factors [18]. Therefore in this section we will be dealing with the H-polarization only. The modification of the above presented data to the case of other than air host medium is straightforward: free-space wavenumber must be re-scaled with the factor $v_{host}^{1/2}$.

In Fig. 9, we present the spectra of the normalized extinction cross-section (that is the sum of TSCS and ACS) for the inclined incidence ($\beta = 45^\circ$) of the H-polarized plane wave

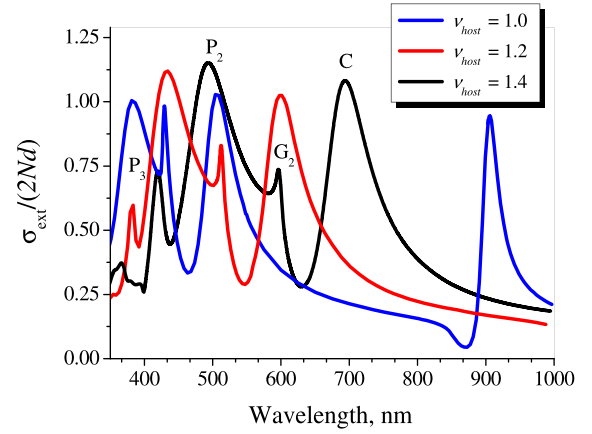


Fig. 9. H-polarization. Normalized extinction cross-section as a function of the wavelength for the grating of $N = 50$ silver strips ($d = 300$ nm, $h = 50$ nm, $p = 500$ nm) for different values of the refractive index of host medium, $v_{host} = 1, 1.2$ and 1.4 ($\beta = 45^\circ$).

on the grating of $N = 50$ silver nanostrips ($d = 300$ nm, $h = 50$ nm and $p = 500$ nm). Here, three different values of the refractive index of the surrounding medium are taken: $v_{host} = 1$ (blue curve), 1.2 (red), and 1.4 (black).

As one can see, all resonance peaks get red-shifted with increasing the refractive index. Besides, in the case of free space, the extinction spectrum demonstrates four resonances: P_2 (384.2 nm), G_2 (428.7 nm), C (506.5 nm), and G_1 (858.3 nm), while for $v_{host} = 1.4$ the GM resonance of the 1-st order (G_1) is shifted beyond the considered wavelength range however the 3-rd order LSP resonance appears at 419.1 nm.

In the engineering of the optical biosensors, two values characterizing their performance are in use: the sensitivity and the figure-of merit (FOM) [4], [5], [17], [32], [33]. The bulk refractive index sensitivity $S_{bulk} = \Delta\lambda_{res}/\Delta v_{host}$ of the optical resonance corresponds to the resonance wavelength shift $\Delta\lambda_{res}$ obtained for the refractive index Δv_{host} variation. Here, it should be noted that the bulk sensitivity of the GM resonance of the m -th order does not depend on the refractive index changes and can be obtained, in the main term, from eq. (2),

$$S_{bulk} = \frac{\Delta\lambda_{G_m}}{\Delta v_{host}} = \frac{\lambda_{G_m}^{(v_{host})} - \lambda_{G_m}^{(air)}}{v_{host} - 1} \approx \frac{p(1 \pm \cos\beta)}{m}, \quad m = 1, 2, \dots \quad (3)$$

The FOM is defined as follows [5], [17]:

$$FOM = S_{bulk}(FWHM)^{-1}, \quad (4)$$

where FWHM is the full width at half maximum of the peak.

As visible from Fig. 9, all resonances of extinction cross-sections are asymmetric Fano resonances. This complicates the quantification of the line-width of each of them. As a remedy, the extinction spectrum can be fitted with an analytical Fano formula [34] (see Appendix A2). The Fano fitting parameters for $v_{host} = 1.4$ are presented in Table 1 and the corresponding fitted curve is shown in Fig. 10 by dots. Note that refractive

TABLE I
FANO FITTING PARAMETERS

Resonance type	ω [THz]	Γ [THz]	q	A
C	438.2	44.8	0.28	0.89
G_2	498.9	21.4	-0.45	0.34
P_2	622.2	135.6	0.22	1.39
P_3	712.8	47.9	-0.19	0.73

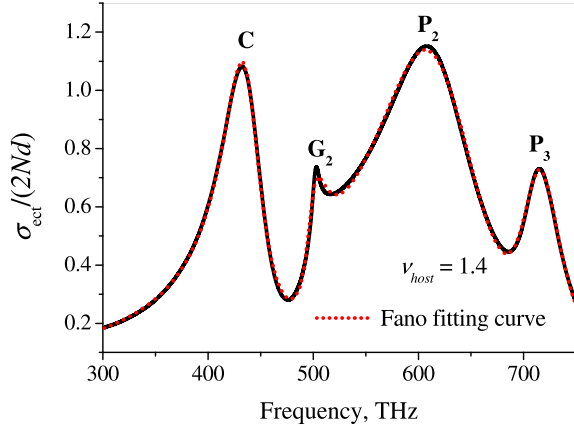


Fig. 10. Normalized extinction spectrum for the grating of $N = 50$ silver strips ($d = 300$ nm, $h = 50$ nm and $p = 500$ nm) in the medium with $\nu_{host} = 1.4$ calculated using GBC-SIE (solid curve) and the Fano fitting curve (dotted).

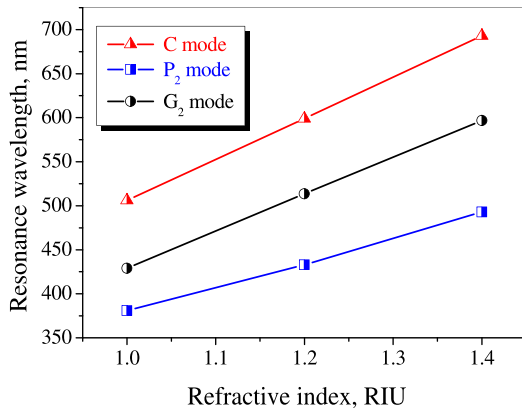


Fig. 11. Resonance wavelengths as a function of the refractive index of the surrounding medium for the same grating as in Fig. 10. Mode types are explained in the inset.

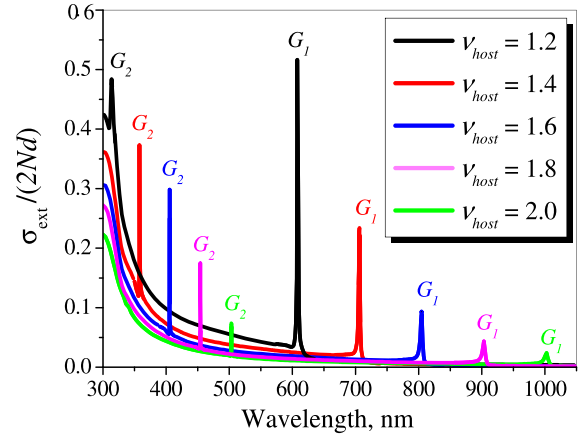
index close to 1.4 corresponds to a typical sensing scenario of the water solution of proteins [5].

In Fig. 11 we show the bulk refractive index sensitivities of three resonances: C (red line), P_2 (blue) and G_2 (black). As can be seen, the resonance wavelength shift dependences are linear. The corresponding data calculated with the aid of Figs. 9, 11 are collected in Table 2. Here the highest bulk sensitivity is 467.5 nm/RIU for the cavity-mode resonance and the lowest is 280 nm/RIU for the LSP-mode resonance of the 2nd order. Still the second-order grating-mode resonance G_2 shows the largest value of FOM, 16.2 RIU⁻¹, which is 6 times larger than FOM of the P_2 resonance, 2.7 RIU⁻¹.

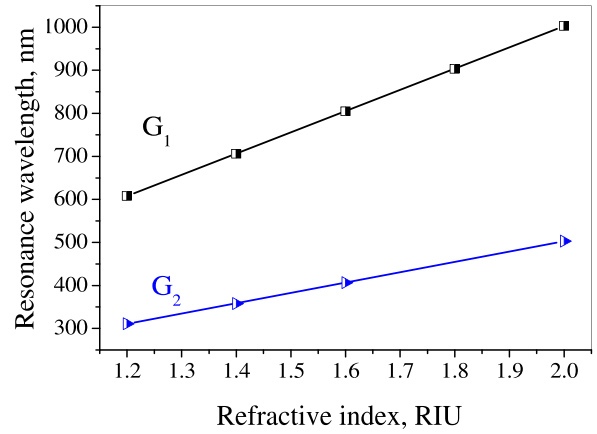
It is also interesting to see that, as follows from the data presented in Fig. 12 (a), the growth of the refractive index

TABLE II
REFRACTIVE-INDEX SENSITIVITY AND FOM
OF THE C, G_2 AND P_2 RESONANCES

Resonance type	S_{bulk} [nm/RIU]	FWHM [nm]	FOM [RIU ⁻¹]
C	467.5	70	6.7
G_2	419.5	26	16.2
P_2	280	105	2.7



(a)



(b)

Fig. 12. (a) The normalized TSCS as a function of the wavelength (a) and the GM-resonance wavelengths of the 1st and 2nd orders as a function of refractive index of the host medium (b) for the H-polarized plane wave normal incidence ($\beta = 90^\circ$) on the grating of $N = 50$, $d = 300$ nm, $h = 50$ nm and $p = 500$ nm.

of the surrounding medium over $\nu_{host} = 1.8$ spoils both the Q-factors (i.e. the FWHM values) and the peak intensities of the GM-resonances of both the first and the second order.

The comparison of the bulk sensitivity and FOM of the GM-resonances of different orders (Table 3) demonstrates that the G_1 -resonance is almost 2 times more sensitive to the refractive-index changes than the G_2 -resonance. Besides, the FOM value of the latter one is 1.5 times higher than of the former. Note that here FWHM value is calculated for a fixed refractive index of host medium, $\nu_{host} = 1.4$.

Note that most of the data presented in the paper have been computed for the grating period of 500 nm. This value was chosen after certain preliminary computations that had shown what combination of the grating parameters was most

TABLE III
REFRACTIVE-INDEX SENSITIVITY AND FOM OF
THE G_1 AND G_2 RESONANCES ($N = 50$)

Resonance type	S_{bulk} [nm/RIU]	FWHM [nm]	FOM [RIU ⁻¹]
G_1	493.1	2.3	214.4
G_2	240.5	1.2	343.6

beneficial to analyze all resonances. In particular, as at the GM resonance the period is almost equal (at the normal incidence) to the wavelength, and we want the wavelength to be in the visible, period of some value between 400 and 800 is reasonable. If this value changes, the GM resonance position moves accordingly – this, in fact, is illustrated by the color map of TSCS in Fig. 5 (d) where the vertical axis is for the period changing from 300 to 650 nm.

VI. CONCLUSIONS

The optical response of the comb-like finite grating made of silver nanostrips has been investigated in the H- and E-waves scattering regimes. In the H-polarization, three different types of optical resonances have been observed and analyzed: LSP-mode resonances on each strip's boundary, CM resonances in the space between adjacent strips, and periodicity-induced GM resonances, which transform to the Bragg-effect resonances if the plane wave comes at the grazing incidence. The GM-resonances, unlike all others, exist in the vicinities of the corresponding Rayleigh anomalies and split into different classes of symmetry. Their interplay depends on the angle of incidence, the period of the grating, and the width and thickness of each strip.

In the E-polarized plane wave scattering, it has been demonstrated that although the metal-strip gratings do not support LSP resonances in the optical range, in the vicinities of the Rayleigh anomalies a rather sharp suppression in both the scattering and absorption is observed. Under the edge-on incidence, one of two families of RA transform to the Bragg-effect resonances similarly to the H-case.

Thus, choosing the comb-like strip grating parameters in optimal manner may help design periodic nanosensors, nanoabsorbers, and surface-enhanced Raman scattering substrates with improved characteristics.

Finally, the bulk sensitivities and the figures-of-merit of all optical resonances appearing under the H-polarized plane-wave illumination on the finite comb-like silver strip gratings have been accurately quantified. It has been shown that the CM-resonances are more sensitive to the bulk refractive-index changes than the others. We have also found that the bulk sensitivities of the GM-resonances are proportional to the grating period and do not depend, in the main term, on the refractive-index of the surrounding medium. What appears important for the sensing applications, the GM-resonances display much higher FOM values than the optical resonances on LSP and cavity modes. This value is mostly determined by the number of the elements in the grating.

The other important issue is fabrication, which can be hard for such geometry with strip vertical-to-horizontal dimension ratio as large as 6:1. Still we believe that even if at present such

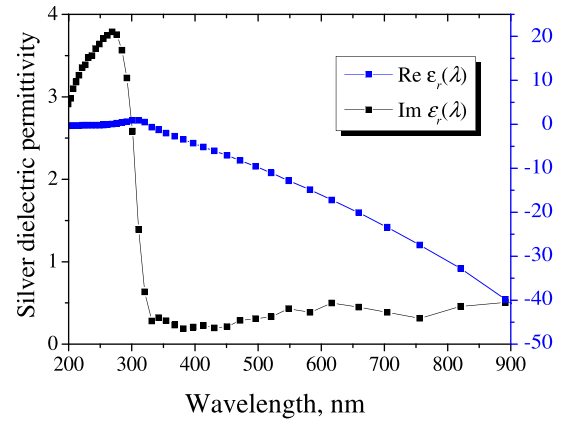


Fig. 13. Real and imaginary parts of the silver permittivity as a function of the wavelength.

“deep” gratings are at the edge of existing molecular beam epitaxy and etching technologies they can become routine in future and hence advance knowledge of their properties is important.

APPENDIX A1

COMPLEX DIELECTRIC FUNCTION OF SILVER

Silver is a noble metal characterized with complex-valued dielectric permittivity, the real part of which is negative in the optical range. This is explained by the fact that at such high frequencies the main contribution to permittivity is provided by the free-electron plasma. Both real and imaginary parts of ε_{Ag} strongly depend on frequency but not on the shape of particle provided that its minimum dimension exceeds 3 nm and hence non-local effects can be neglected [23]. As relative magnetic permeability remains equal to 1, such a material is also known as “negative dielectric”.

To characterize the complex dielectric function of silver, in the simulations $\varepsilon_{Ag}(\lambda)$ is frequently approximated using the Drude formula with fitted parameters. However this formula is able to reproduce only the real part of permittivity while the imaginary part remains heavily erroneous. Modifications of Drude formula can suffer of non-physical negative values of the imaginary part of epsilon [35].

Therefore we took the experimental data (measured at discrete wavelength) of [24] and used an Akima cubic spline interpolation to eliminate the wiggles in the interpolant. The wavelength dependences of real and imaginary parts of silver on the wavelength in the visible range are shown in Fig. 13.

APPENDIX A2

FANO FITTING MODEL

In contrast to classical Lorentzian resonances, the Fano resonance exhibits a distinctly asymmetric shape of spectrum. As found by Fano, it can be fitted with analytical formula [34],

$$\sigma_{\text{ext}}(\omega) = A_0 + \sum_j A_j \frac{(q_j \Gamma_j / 2 + E - E_j)^2}{(E - E_j)^2 + (\Gamma_j / 2)^2}, \quad (\text{A2})$$

where $E_j = \hbar\omega_j$ is the energy (\hbar is the Planck constant), ω_j is frequency, q_j is the phenomenological shape parameter (or Fano asymmetry parameter) of the j -th resonance

mode, Γ_j describes the corresponding resonance FWHM, and A_0 , A_j are the fitting constant factors.

ACKNOWLEDGEMENTS

The author would like to thank J. Ctyroky, R. Sauleau, and A. I. Nosich for many fruitful discussions and encouragement.

REFERENCES

- [1] D. R. Fredkin and I. D. Mayergoyz, "Resonant behavior of dielectric objects (electrostatic resonances)," *Phys. Rev. Lett.*, vol. 91, pp. 253902–253905, Dec. 2003.
- [2] T. Søndergaard and S. I. Bozhevolnyi, "Strip and gap plasmon polariton optical resonators," *Phys. Status Solidi B*, vol. 245, no. 1, pp. 9–19, 2008.
- [3] A. Christ, T. Zentgraf, J. Kuhl, S. G. Tikhodeev, N. A. Gippius, and H. Giessen, "Optical properties of planar metallic photonic crystal structures: Experiment and theory," *Phys. Rev. B*, vol. 70, no. 12, pp. 125113–125128, 2004.
- [4] J. Homola, "Surface plasmon resonance sensors for detection of chemical and biological species," *Chem. Rev.*, vol. 108, no. 2, pp. 462–493, 2008.
- [5] A. Murphy *et al.*, "Fabrication and optical properties of large-scale arrays of gold nanocavities based on rod-in-a-tube coaxials," *Appl. Phys. Lett.*, vol. 102, no. 10, pp. 103103-1–103103-5, Mar. 2013.
- [6] K. T. Carron, W. Fluhr, M. Meier, A. Wokaun, and H. W. Lehmann, "Resonances of two-dimensional particle gratings in surface-enhanced Raman scattering," *J. Opt. Soc. Amer. B*, vol. 3, no. 3, pp. 430–440, 1986.
- [7] S. Peng and G. M. Morris, "Resonant scattering from two-dimensional gratings," *J. Opt. Soc. Amer. A*, vol. 13, no. 5, pp. 993–1005, 1996.
- [8] S. Zou, N. Janel, and G. C. Schatz, "Silver nanoparticle array structures that produce remarkably narrow plasmon lineshapes," *J. Chem. Phys.*, vol. 120, no. 23, pp. 10871-1–10871-5, 2004.
- [9] R. Gomez-Medina, M. Laroche, and J. J. Sáenz, "Extraordinary optical reflection from sub-wavelength cylinder arrays," *Opt. Exp.*, vol. 14, no. 9, pp. 3730–3737, 2006.
- [10] T. L. Zinenko and A. I. Nosich, "Plane wave scattering and absorption by flat gratings of impedance strips," *IEEE Trans. Antennas Propag.*, vol. 54, no. 7, pp. 2088–2095, Jul. 2006.
- [11] D. M. Natarov, V. O. Byelobrov, R. Sauleau, T. M. Benson, and A. I. Nosich, "Periodicity-induced effects in the scattering and absorption of light by infinite and finite gratings of circular silver nanowires," *Opt. Exp.*, vol. 19, no. 22, pp. 22176–22190, 2011.
- [12] P. Ghenuche *et al.*, "Optical extinction in a single layer of nanorods," *Phys. Rev. Lett.*, vol. 109, pp. 143903-1–143903-5, Oct. 2012.
- [13] T. V. Teperik and A. Degiron, "Design strategies to tailor the narrow plasmon-photonic resonances in arrays of metallic nanoparticles," *Phys. Rev. B*, vol. 86, pp. 245425-1–245425-5, Dec. 2012.
- [14] S. R. K. Rodriguez, M. C. Schaafsma, A. Berrier, and J. G. Rivas, "Collective resonances in plasmonic crystals: Size matters," *Phys. B, Condens. Matter*, vol. 407, no. 20, pp. 4081–4085, 2012.
- [15] D. M. Natarov, R. Sauleau, and A. I. Nosich, "Periodicity-enhanced plasmon resonances in the scattering of light by sparse finite gratings of circular silver nanowires," *IEEE Photon. Technol. Lett.*, vol. 24, no. 1, pp. 43–45, Jan. 1, 2012.
- [16] V. O. Byelobrov, T. M. Benson, and A. I. Nosich, "Binary grating of subwavelength silver and quantum wires as a photonic-plasmonic lasing platform with nanoscale elements," *IEEE J. Sel. Topics Quantum Electron.*, vol. 18, no. 6, pp. 1839–1846, Nov./Dec. 2012.
- [17] B. Špačková and J. Homola, "Sensing properties of lattice resonances of 2D metal nanoparticle arrays: An analytical model," *Opt. Exp.*, vol. 21, no. 22, pp. 27490–27502, 2013.
- [18] T. L. Zinenko, M. Marciniak, and A. I. Nosich, "Accurate analysis of light scattering and absorption by an infinite flat grating of thin silver nanostrips in free space using the method of analytical regularization," *IEEE J. Sel. Topics Quantum Electron.*, vol. 19, no. 3, May/Jun. 2013, Art. ID 9000108.
- [19] O. V. Shapoval, R. Sauleau, and A. I. Nosich, "Modeling of plasmon resonances of multiple flat noble-metal nanostrips with a median-line integral equation technique," *IEEE Trans. Nanotechnol.*, vol. 12, no. 3, pp. 442–449, May 2013.
- [20] D. M. Natarov, R. Sauleau, M. Marciniak, and A. I. Nosich, "Effect of periodicity in the resonant scattering of light by finite sparse configurations of many silver nanowires," *Plasmonics*, vol. 9, no. 2, pp. 389–407, 2014.
- [21] D. M. Natarov, M. Marciniak, R. Sauleau, and A. I. Nosich, "Seeing the order in a mess: Optical signature of periodicity in a cloud of plasmonic nanowires," *Opt. Exp.*, vol. 22, no. 23, pp. 28190–28198, 2014.
- [22] V. O. Byelobrov, T. L. Zinenko, and A. I. Nosich, "Periodicity matters: Grating or lattice resonances in the scattering by sparse arrays of sub-wavelength strips and wires," *IEEE Antennas Propag. Mag.*, vol. 57, 2015.
- [23] O. J. F. Martin, "Plasmon resonances in nanowires with a non-regular cross-section," in *Optical Nanotechnologies (Topics in Applied Physics)*, vol. 88, J. Tominaga and D. P. Tsai, Eds. Berlin, Germany: Springer-Verlag, 2003, pp. 183–210.
- [24] P. B. Johnson and R. W. Christy, "Optical constants of the noble metals," *Phys. Rev. B*, vol. 6, pp. 4370–4378, Dec. 1972.
- [25] I. O. Sukharevsky, O. V. Shapoval, A. Altintas, and A. I. Nosich, "Validity and limitations of the median-line integral equation technique in the scattering by material strips of sub-wavelength thickness," *IEEE Trans. Antennas Propag.*, vol. 62, no. 7, pp. 3623–3631, Jul. 2014.
- [26] K. M. Mitzner, "Effective boundary conditions for reflection and transmission by an absorbing shell of arbitrary shape," *IEEE Trans. Antennas Propag.*, vol. 16, no. 6, pp. 706–712, Nov. 1968.
- [27] E. H. Bleszynski, M. Bleszynski, and T. Jaroszewicz, "Surface-integral equations for electromagnetic scattering from impenetrable and penetrable sheets," *IEEE Antennas Propag. Mag.*, vol. 35, no. 6, pp. 14–25, Dec. 1993.
- [28] M. V. Balaban, E. I. Smotrova, O. V. Shapoval, V. S. Bulygin, and A. I. Nosich, "Nystrom-type techniques for solving electromagnetics integral equations with smooth and singular kernels," *Int. J. Numer. Model., Electron. Netw., Devices, Fields*, vol. 25, nos. 5–6, pp. 490–511, 2012.
- [29] O. V. Shapoval, J. Čtyroky, and A. I. Nosich, "Resonance effects in the optical antennas shaped as finite comb-like gratings of noble-metal nanostrips," *Proc. SPIE*, vol. 8781, pp. 87810U-1–87810U-8, May 2013.
- [30] L. Rayleigh, "On the dynamical theory of gratings," *Proc. Roy. Soc. London, A, Containing Papers Math. Phys. Character*, vol. 79, no. 532, pp. 399–416, 1907.
- [31] A. Yariv, *Optical Electronics in Modern Communications*. New York, NY, USA: Oxford Univ. Press, 1997.
- [32] P. Offermans *et al.*, "Universal scaling of the figure of merit of plasmonic sensors," *ACS Nano*, vol. 5, no. 6, pp. 5151–5157, 2011.
- [33] E. A. Velichko and A. I. Nosich, "Refractive-index sensitivities of hybrid surface-plasmon resonances for a core-shell circular silver nanotube sensor," *Opt. Lett.*, vol. 38, no. 23, pp. 4978–4981, 2013.
- [34] U. Fano, "Effects of configuration interaction on intensities and phase shifts," *Phys. Rev.*, vol. 124, no. 6, pp. 1866–1878, 1961.
- [35] D. M. Natarov, "Modes of core-shell silver wire plasmonic nanolaser beyond Drude formula," *J. Opt.*, vol. 16, no. 7, pp. 075002-1–075002-6, 2014.



Olga V. Shapoval (S'10–M'15) was born in Nikopol, Ukraine, in 1987. She received the M.S. (Hons.) degree in applied mathematics from Kharkiv National University, in 2009, and the Ph.D. degree in radio physics from the Institute of Radio-Physics and Electronics, National Academy of Sciences of Ukraine, in 2014, where she is currently a Junior Scientist with the Laboratory of Micro and Nano Optics.

Dr. Shapoval was a recipient of the International Union for Radio Science (URSI) Young Scientist Award for attending the Asia-Pacific Radio Science Conference in Toyama and the Doctoral Research Award from the IEEE Antennas and Propagation Society, in 2010. In 2012, she received the Ph.D. Scholarship from the International Visegrad Fund. In 2013, she was also a recipient of the URSI Young Scientist Award for attending the Electromagnetic Theory Symposium in Hiroshima, and the Young Scientist Grant from the TICRA Foundation, Denmark, in 2014.